2014-02-11

Myosin-binding protein C displaces tropomyosin to activate cardiac thin filaments and governs their speed by an independent mechanism

Ji Young Mun
University of Massachusetts Medical School

Et al.

Myosin-binding protein C displaces tropomyosin to activate cardiac thin filaments and governs their speed by an independent mechanism

Ji Young Mun[a,1], Michael J. Previs[b,1], Hope Y. Yu[b], James Gulick[c], Larry S. Tobacman[d], Samantha Beck Previs[b], Jeffrey Robbins[c], David M. Warshaw[b,2], and Roger Craig[a,2]

[a]Department of Cell and Developmental Biology, University of Massachusetts Medical School, Worcester, MA 01655; [b]Department of Molecular Physiology and Biophysics, University of Vermont, Burlington, VT 05405; [c]Division of Molecular Cardiovascular Biology, Cincinnati Children's Hospital Medical Center, Cincinnati, OH 45229; and [d]Department of Medicine, University of Illinois at Chicago, Chicago, IL 60612

Edited by Clara Franzini-Armstrong, University of Pennsylvania Medical Center, Philadelphia, PA, and approved January 3, 2014 (received for review August 23, 2013)

Myosin-binding protein C (MyBP-C) is an accessory protein of striated muscle thick filaments and a modulator of cardiac muscle contraction. Defects in the cardiac isoform, cMyBP-C, cause heart disease. cMyBP-C includes 11 Ig- and fibronectin-like domains and a cMyBP-C-specific motif. In vitro studies show that in addition to binding to the thick filament via its C-terminal region, cMyBP-C can also interact with actin via its N-terminal domains, modulating thin filament motility. Structural observations of F-actin decorated with N-terminal fragments of cMyBP-C suggest that cMyBP-C binds to actin close to the low Ca^{2+} binding site of tropomyosin. This suggests that cMyBP-C might modulate thin filament activity by interfering with tropomyosin regulatory movements on actin. To determine directly whether cMyBP-C binding affects tropomyosin position, we have used electron microscopy and in vitro motility assays to study the structural and functional effects of N-terminal fragments binding to thin filaments. 3D reconstructions suggest that under low Ca^{2+} conditions, cMyBP-C displaces tropomyosin toward its high Ca^{2+} position, and that this movement corresponds to thin filament activation in the motility assay. At high Ca^{2+}, cMyBP-C had little effect on tropomyosin position and caused slowing of thin filament sliding. Unexpectedly, a shorter N-terminal fragment did not displace tropomyosin or activate the thin filament at low Ca^{2+} but slowed thin filament sliding as much as the larger fragments. These results suggest that cMyBP-C may both modulate thin filament activity, by physically displacing tropomyosin from its low Ca^{2+} position on actin, and govern contractile speed by an independent molecular mechanism.

muscle regulation | muscle activation

Myosin-binding protein C (MyBP-C) is an accessory protein of vertebrate striated muscle thick filaments (1) that is known to modulate cardiac muscle contraction (2). The skeletal isoform includes 10 Ig-like (Ig) and fibronectin type 3-like (Fn) domains, numbered C1 through C10 from the N terminus, together with a MyBP-C-specific motif (the M-domain) between C1 and C2 and a Pro-Ala-rich sequence at the N terminus. The cardiac isoform (cMyBP-C) has an additional N-terminal Ig domain (C0), four phosphorylation sites in the M-domain, and a 28-residue insert in the C5 domain (3) (Fig. 1). MyBP-C binds to the thick filament in the C-zone of the sarcomeric A-band (4) via its C-terminal domains (C8–C10) (5), whereas its N-terminal region contains binding sites for myosin S2 (6-10) and the myosin regulatory light chain (11).

In addition to binding to myosin, MyBP-C also interacts with actin (12) and with thin filaments (13) via its N-terminal region (9, 10, 14–17; cf. 18). In the in vitro motility assay, actin filament sliding over myosin is slowed by N-terminal fragments of cMyBP-C to the same extent as whole cMyBP-C (19), possibly by slowing the myosin detachment rate from actin (19) or tethering the thick to the thin filament (16, 19). In an assay closer to the in vivo situation, the sliding of F-actin over native cardiac thick filaments was slowed specifically in the C-zone, and this slowing was ablated by removal of C0C1 and the first 17 amino acids of the M-domain [known as C0C1f (16); Fig. 1] (20). On the basis of yeast 2 hybrid experiments, it was concluded that the C1 and M domains were necessary for actin binding and that replacement of endogenous cMyBP-C with actin binding-ablated cMyBP-C resulted in its abnormal sarcomeric distribution and disturbance of the sarcomeric structure (9). These in vitro demonstrations of actin binding are supported by electron tomographic observations showing MyBP-C extending from the thick to the thin filaments in the intact sarcomere, consistent with a model in which the N terminus of MyBP-C binds to the thin filament (21, 22). Together, these results suggest that actin binding is physiologically relevant and that the slowing of actin filament sliding is one possible mechanism by which cMyBP-C modulates cardiac contractility (5, 23, 24).

The structural basis of cMyBP-C's N-terminal binding to F-actin has been studied in several ways. Neutron scattering and NMR titration analysis of F-actin decorated with the N-terminal fragment C0C2 (Fig. 1) suggested that C0C2 binds to subdomain 1 (SD1) and the DNase loop of actin (25) via key regions within C0 and C1 (10). More direct observations by negative stain electron microscopy (26) and 3D reconstruction (27) suggest that C0 and C1 bind to SD1 of actin, whereas the M domain crosses

Significance

Myosin-binding protein C (MyBP-C) is a component of myosin filaments, one of the two sets of contractile elements whose relative sliding is the basis of muscle contraction. In the heart, MyBP-C modulates contractility in response to cardiac stimulation; mutations in MyBP-C lead to cardiac disease. The mechanism by which MyBP-C modulates cardiac contraction is not understood. Using electron microscopy and a light microscopic assay for filament sliding, we demonstrate that MyBP-C binds to the other set of filaments, containing actin and the regulatory component, tropomyosin. In so doing, it displaces tropomyosin from its inhibitory position to activate actin filament interaction with myosin, promoting filament sliding. These findings provide insights into the molecular basis of heart function.

Author contributions: J.Y.M., M.J.P., D.M.W., and R.C. designed research; J.Y.M., M.J.P., H.Y.Y., and S.B.P. performed research; J.G., L.S.T., and J.R. contributed new reagents/analytic tools; J.Y.M., M.J.P., H.Y.Y., S.B.P., D.M.W., and R.C. analyzed data; and J.Y.M., M.J.P., D.M.W., and R.C. wrote the paper.

The authors declare no conflict of interest.

This article is a PNAS Direct Submission.

[1]J.Y.M. and M.J.P. contributed equally to this work.

[2]To whom correspondence may be addressed. E-mail: roger.craig@umassmed.edu or david.warshaw@uvm.edu.

This article contains supporting information online at www.pnas.org/lookup/suppl/doi:10.1073/pnas.1316001111/-/DCSupplemental.

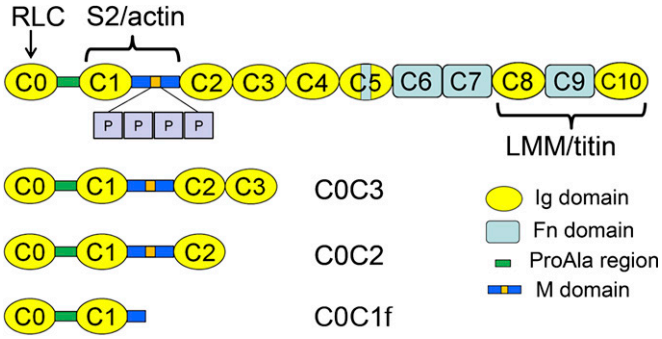

Fig. 1. Schematic of cMyBP-C and the expressed N-terminal fragments C0C3, C0C2, and C0C1f used in this study. cMyBP-C consists of 8 Ig and 3 Fn domains together with a cMyBP-C-specific M-domain, containing a phosphorylation region (orange) with 4 phosphorylatable serines (P), a ProAla-rich domain, and a cardiac-specific insert (blue) in the C5 domain.

over SD2, possibly binding to the next SD1, and C2 and C3 lie above the surface of the filament (27, 28).

The position of cMyBP-C binding on actin SD1 suggests that in addition to inhibiting actomyosin interactions, it might also affect thin filament regulation by interfering with the binding of tropomyosin/troponin (Tm/Tn) to actin. Tm and Tn regulate muscle contraction by movement of Tm in response to calcium binding by Tn (29). At low Ca^{2+}, Tm lies on SD1, where it sterically blocks the binding of myosin to actin (the "blocked" position); the consequent inhibition of actin-myosin interaction leads to muscle relaxation. On activation, Tn binds Ca^{2+}, causing Tm to move onto actin SD3 (the "closed" position), exposing myosin binding sites on SD1 and initiating crossbridge cycling and contraction (29–35). When a model of Tm in its low Ca^{2+} (blocked) state is positioned on the reconstruction of F-actin decorated with C0C3, it appears to clash with cMyBP-C's C0 and C1 domains, suggesting that cMyBP-C and Tm might compete for binding to SD1 in the relaxed thin filament (25, 27, 28). As a consequence, cMyBP-C might be expected to activate the thin filament by physically preventing Tm from assuming its blocked position (25, 27, 28). Motility (19) and solution kinetics studies (36, 37) support this concept, showing that the N-terminal C1C2 fragment activates thin filaments in low Ca^{2+} similarly to rigor heads.

Here we have investigated cMyBP-C's potential to modulate cardiac contractility by contrasting mechanisms; that is, activating the thin filament and inhibiting maximal actomyosin mechanical activity. First we used negative-staining EM and 3D reconstruction to investigate whether cMyBP-C displaces Tm at low Ca^{2+}, by decorating regulated thin filaments (containing F-actin, Tm and Tn) with C0C2. In parallel experiments, we determined the functional consequences of such N-terminal fragments on regulated thin filament activation and sliding velocities in an in vitro motility assay. We find clear structural evidence for displacement of Tm toward the high Ca^{2+} (closed) position when C0C2 binds to thin filaments under low Ca^{2+} conditions, suggesting that N-terminal binding should activate the thin filament; this was confirmed in the motility assay. We also demonstrate that C0C2 has no effect on Tm position under high Ca^{2+} conditions but inhibits maximal sliding velocity in the motility assay. Interestingly, a smaller fragment (C0C1f; Fig. 1) binds to the thin filament under low Ca^{2+} conditions but does not displace Tm or activate thin filament sliding. However, C0C1f still inhibits thin filament sliding at high Ca^{2+} to the same extent as the larger N-terminal fragment. These results suggest that cMyBP-C may play two physiological roles in intact muscle, displacing Tm from the "blocked" position at low Ca^{2+} to modulate thin filament activation, and governing maximal sliding velocity at high Ca^{2+} by a potentially independent molecular mechanism.

Results

Negative Staining of Thin Filaments Decorated with C0C2 at Low and High Ca^{2+}. Reconstituted and native thin filaments were mixed with C0C2 (Fig. 1) at molar ratios of 1:6, 1:3, 1:1, or 7:1 (actin:C0C2) in solutions containing KAc (or NaCl) at concentrations from 100 to 180 mM (see *Materials and Methods*). Low Ca^{2+} solutions contained 0.2 mM EGTA, whereas high Ca^{2+} solutions were the same, with Ca^{2+} added to total 0.33 mM [pCa (negative log of calcium concentration), 3.9].

Negatively stained low-Ca^{2+} control (no C0C2 decoration) native (Fig. 2 *A* and *D*) and reconstituted (Figs. S1*A* and S2 *A* and *D*) thin filaments showed typical actin subunits and occasional resolution of Tm strands (31). C0C2 decoration caused a clear increase in filament diameter, most obviously when more C0C2 was added (1:3 and 1:6 ratios of actin:C0C2; Fig. 2 *C* and *F*; Fig. S1*D*; Table S1). In addition, 1:1 and 7:1 molar ratios showed a smaller, but still visible, increase (Fig. 2 *B* and *E*; Figs. S1 *B* and *C* and S2 *B*, *C*, *E*, and *F*; Table S1). Clear decoration was observed in all ionic conditions with no major difference in the level of decoration or background protein. The higher levels of decoration obscured detailed actin and tropomyosin structure. The appearance and diameter of filaments decorated under high Ca^{2+} conditions (Fig. S3) were similar to those at low Ca^{2+}.

Most experiments were carried out by adding C0C2 to native or preformed reconstituted thin filaments. To determine whether Tm and Tn could still bind to actin if C0C2 were bound first, we also reversed the order of mixing. The apparent level of decoration and the filament diameter appeared to be independent of the order of mixing (Fig. S2; Table S1).

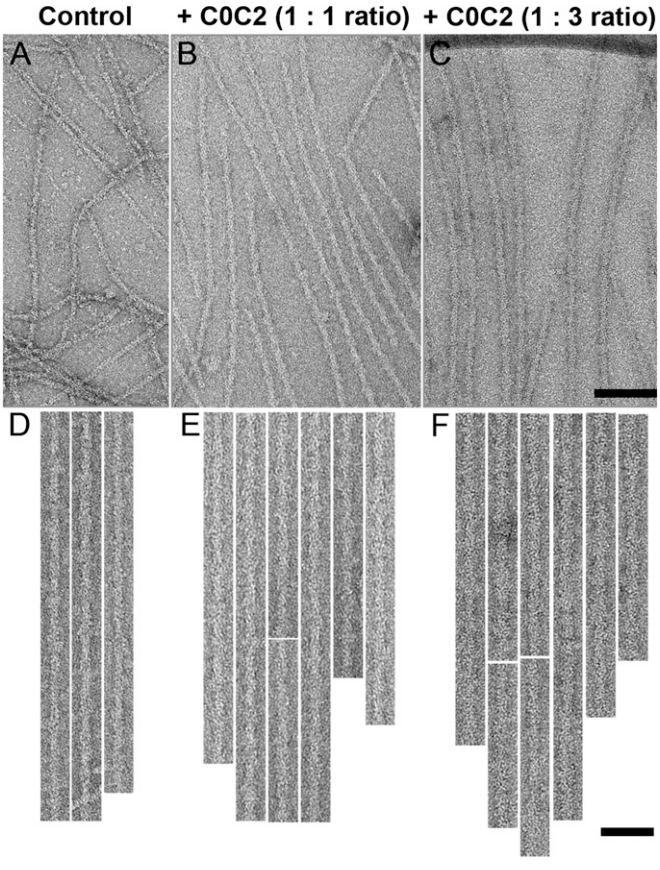

Fig. 2. Decoration of native thin filaments with C0C2 under low Ca^{2+} conditions. (*A*, *D*) Undecorated control. (*B*, *C*, *E*, *F*) Filaments decorated with C0C2 at A:C0C2 molar ratios of 1:1 (*B*, *E*) and 1:3 (*C*, *F*). Filaments in *D*–*F* have been computationally straightened. [Scale bar (*A*–*C*) = 100 nm; (*D*–*F*) = 50 nm.)

3D Reconstruction of Thin Filaments Decorated with C0C2 at Low and High Ca^{2+}. 3D reconstruction of computationally straightened thin filaments was carried out by iterative helical real-space reconstruction (38). Control filaments (no decoration) in low and high Ca^{2+} showed clear actin subunits and elongated Tm strands running along each long-pitch actin helix (Fig. 3). At low Ca^{2+}, Tm is seen to lie near the junction of SD1 and SD3 of actin, over the main myosin-binding site (the blocked position), as found in previous studies (31, 32) (Fig. 3 *A* and *D*). At high Ca^{2+}, Tm moves to the "closed" position on the inner domain of actin, exposing myosin-binding sites on SD1 (Fig. 3 *B* and *E*) (31, 32). The two Tm positions were supported by fitting the reconstructions with molecular models of F-actin-Tm, where Tm is in the blocked or closed position (Fig. 3 *A* and *B*) (39). The change in Tm position induced by Ca^{2+} was especially clear when high and low Ca^{2+} reconstructions were superimposed (Fig. 3 *C* and *F*), confirming that Tm and its well-documented Ca^{2+}-induced movement are clearly seen by our procedures. Similar results were obtained for both native and reconstituted filaments (Fig. 3 *A* and *B*; Figs. S4*B* and S5*B*).

To determine the effect of C0C2 on Tm position under low Ca^{2+} conditions, reconstructions were computed for native filaments decorated with C0C2 at different molar ratios (Fig. 4). All reconstructions again showed clear actin subunits and Tm strands. Actin subunit shape was similar to that in control filaments, especially at the lower levels of decoration. At higher levels, the binding of C0C2 was visualized as an extra density on SD1 of actin (Fig. 4*F*, arrows), similar to its binding position observed previously (27, 28).

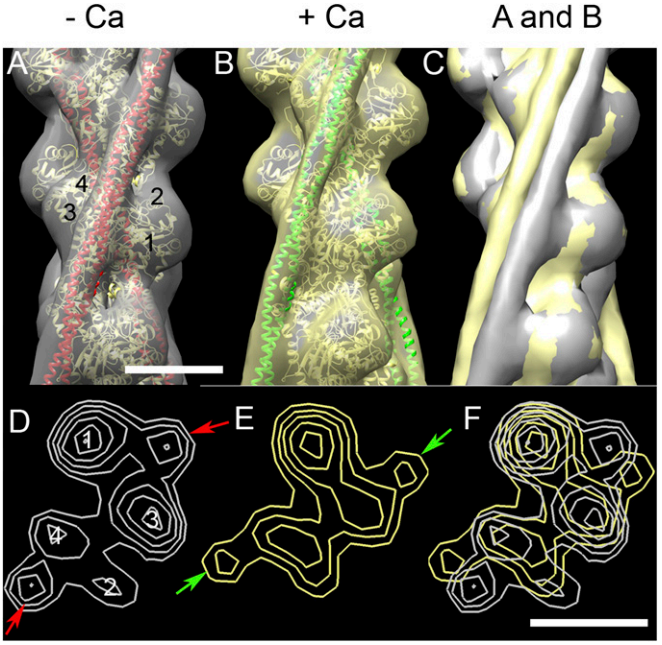

Fig. 3. 3D reconstructions of native control thin filaments under low and high Ca^{2+} conditions. (*A*) Low Ca^{2+} filament (gray surface rendering) fitted with ribbon depiction of low-Ca^{2+} A.Tm atomic model (39) (actin monomers, yellow; Tm, red). (*B*) High-Ca^{2+} reconstruction (yellow surface rendering), fitted with high-Ca^{2+} A.Tm atomic model (actin monomers, yellow; Tm, green). (*C*) Superposition of *A* and *B* demonstrating Tm shift on to inner domain of actin at high Ca^{2+} (note: slight variations in actin contours in *A* and *B* cause either gray or yellow to appear on the actin surface in *C*). (*D* and *E*) Transverse sections of low and high Ca^{2+} reconstructions, respectively, showing positioning of Tm (arrows) near the junction of actin SD1 and SD3 in low Ca^{2+}, and on SD3 in high Ca^{2+}. (*F*) Superposition of *D* and *E*, demonstrating the shift of Tm. Filaments in *A*–*C* oriented with pointed end at top; actin subdomains are marked in *A* and *D*. (Scale bar = 5 nm.)

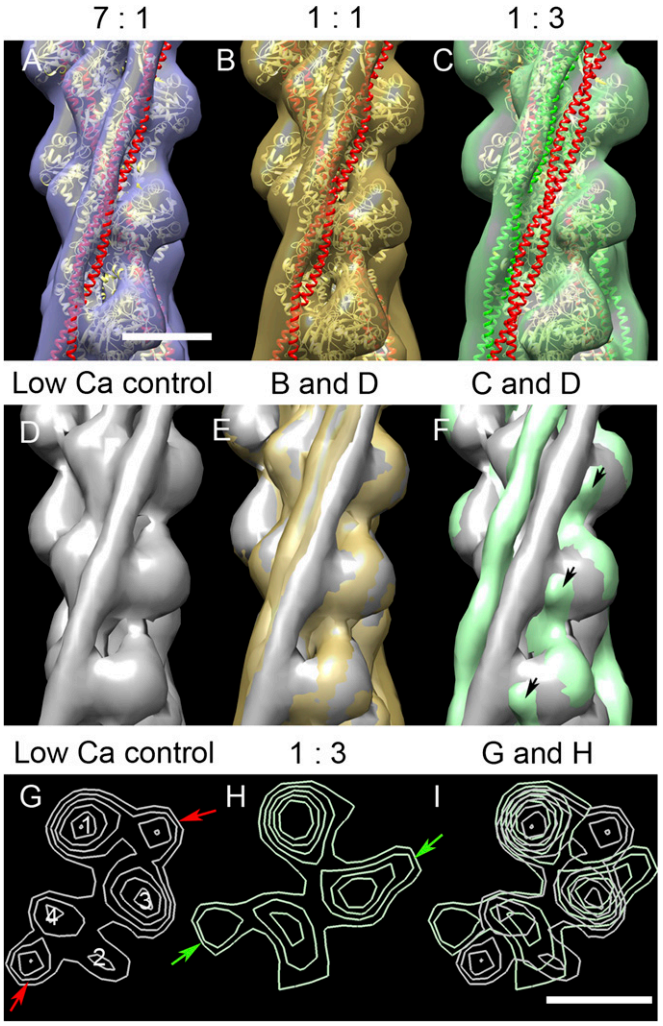

Fig. 4. 3D reconstructions of native thin filaments decorated with C0C2 under low Ca^{2+} conditions. (*A*–*C*) Reconstructions with the indicated ratios of A:C0C2 fitted with A.Tm atomic models (39), as in Fig. 3, with Tm in blocked (red) or closed (green) position. With low levels of C0C2, there was a small movement of Tm from the blocked position (*A* and *B*), whereas with the highest level, Tm shifted to approximately the closed position (*C*). (*E* and *F*) show superposition of *B* and *C*, respectively, on the low Ca^{2+} control (*D*), demonstrating the smaller and larger shifts; black arrows indicate protrusion on SD1 surface, close to Tm, which we attribute to proximal region of C0C2. (*G* and *H*) Transverse sections of *D* and *C*, respectively, showing the shift of Tm from the blocked position in control (red arrows) to the closed position in C0C2-decorated filament (green arrows). (*I*) Superposition of *G* and *H*. Filaments in *A*–*F* oriented with the pointed end up. (Scale bar = 5 nm.)

The effects of C0C2 binding on Tm position were determined by superimposing decorated and control filament reconstructions (Fig. 4 *D*–*I*) and by fitting of blocked and closed position A.Tm atomic models (39) to the reconstructions (Fig. 4 *A*–*C*). Addition of C0C2 appeared to cause a small movement of Tm in the direction of the closed position when the lower amounts of C0C2 were used (Fig. 4 *A*, *B*, and *E*), and a larger movement, as far as the closed position or slightly further, with the highest amount of C0C2 (Fig. 4 *C*, *F*, and *H*) or when C0C2 was added to F-actin before the addition of Tm.Tn (Fig. S4*D*). These results, showing displacement of Tm from its low-Ca^{2+} position by C0C2, suggest direct competition between C0C2 and Tm for Tm's low-Ca^{2+} binding region on actin. This displacement would be expected to activate the thin filament.

Visibility of C0C2 in the reconstructions varied with conditions. In filaments showing a large Tm shift (high ratios of

C0C2 added and reverse order of addition), C0C2 density appeared stronger than in those showing a smaller shift (lower ratios, normal order; Fig. 4*C* and Fig. S4*D*; compare with Fig. 4 *A* and *B* and Fig. S4*C*). These observations support the view that Tm and C0C2 compete for similar sites on actin. The reconstructions show only the proximal region of C0C2, and we assume that the more distal domains are not well ordered under our experimental conditions.

In high Ca^{2+} conditions, the position of Tm in C0C2-decorated thin filaments was similar to that of control high Ca^{2+} filaments, and clear C0C2 density was visible on SD1 of actin (Fig. S5) in a similar position to that seen in F-actin decorated with C0C2 (27). Thus, C0C2 did not displace Tm from its closed position, suggesting that C0C2 and Tm occupy different binding interfaces on actin at high Ca^{2+}.

3D Reconstruction of Thin Filaments Decorated with C0C1f at Low and High Ca^{2+}. We also studied the effect on Tm position of a shorter fragment (C0C1f; Fig. 1) known to bind to F-actin (16, 27). Filaments decorated with C0C1f were wider than controls, clearly demonstrating binding of the fragment (Fig. S6 *A* and *B*; Table S1). However, 3D reconstructions showed no change in position of Tm compared with controls, either at low (Fig. 5) or high Ca^{2+} (Fig. S7), suggesting that C0C1f would have no activating effect. The site of binding of C0C1f was mainly on the front of actin SD1, although the density was not strong (Figs. 5 and Fig. S7).

Effect of N-Terminal Fragments on Native Thin Filament Sliding at Low and High Ca^{2+}. The sliding of native cardiac thin filaments on mouse cardiac myosin was observed in an in vitro motility assay over a range of Ca^{2+} concentrations (Fig. 6 and Fig. S8). Thin filament sliding was fully regulated by Ca^{2+}, with little to no motion observed at low Ca^{2+} (pCa > 7) and sigmoidal increases in velocity and fraction of filaments moving at higher Ca^{2+} concentrations (Fig. S8, controls). Multiplying the thin filament velocity by the fraction of filaments moving (Fig. S8) gives an effective activation curve with a pCa_{50} of 6.15 ± 0.09 (Fig. 6, control). Although the shorter C0C2 fragment was used in our structural studies (to minimize interference with Tm visibility in the reconstructions), we have shown previously that C0C2 and C0C3 bind similarly to actin filaments (27) and are functionally identical in their inhibition of actin filament motility (16). On addition of 1 μM C0C3 (Fig. 1) to the assay, thin filament sliding was now observed even at the lowest Ca^{2+} level (Fig. S8), and there was a significant shift in pCa_{50} for the effective activation curve to 7.78 ± 0.33 ($P < 0.05$; Fig. 6). At high Ca^{2+}, maximal sliding velocity was inhibited by 50% (Fig. S8), as reported previously for C0C2 (19). In contrast, addition of 1 μM C0C1f showed

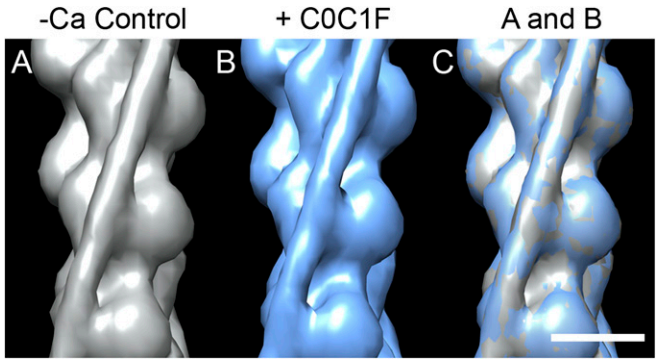

Fig. 5. 3D reconstructions of native thin filaments decorated with C0C1f under low Ca^{2+} conditions. (*A*) Low Ca^{2+} control filament (gray surface rendering). (*B*) C0C1f-decorated filament (blue). (*C*) Superposition of low Ca^{2+} control (*A*) and C0C1f-decorated filament (*B*) showing no Tm shift. (Scale bar = 5 nm.)

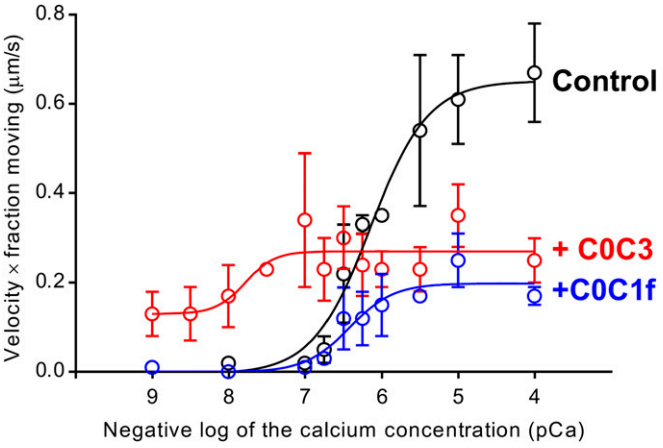

Fig. 6. Effect of N-terminal cMyBP-C fragments on native thin filament sliding in in vitro motility assays. The graph shows "effective activation" (thin filament velocity × fraction of filaments moving) vs. pCa. The black line shows native thin filaments demonstrating a sigmoidal response to Ca^{2+}. The red line shows C0C3 activated the thin filaments at low Ca^{2+}, increased Ca^{2+} sensitivity, and inhibited maximal velocity. The blue line shows C0C1f had no effect on activation or Ca^{2+} sensitivity but inhibited maximal velocity. See Fig. S8 for individual velocity and fraction-moving data.

no activation of the thin filament at low calcium (Fig. S8) and no change in pCa_{50} for the effective activation curve (6.42 ± 0.15; $P > 0.05$; Fig. 6) but showed inhibition of maximal velocity by 47% at higher Ca^{2+} concentrations, similar to C0C3 (Fig. S8). The inability of C0C1f to activate the thin filament despite retaining its inhibitory capacity suggests that thin filament activation and inhibition of maximal velocity may be governed by two independent molecular mechanisms.

Discussion

Elimination of MyBP-C from muscle fibers by chemical extraction or genetic ablation results in changes to the muscle's Ca^{2+} sensitivity of force production (40–42), to its shortening velocity (43, 44), and to the kinetics of tension recovery after stretch (45). These alterations emphasize the physiological roles played by MyBP-C in both Ca^{2+}-dependent muscle activation and in modulation of cardiac contractility. However, the structural basis for these distinct functions has not been determined. Using a combination of structural and molecular functional assays, we have shown that the N terminus of cMyBP-C displaces Tm to activate native thin filaments at low Ca^{2+} and slows thin filament sliding velocity at high Ca^{2+}, presumably through independent molecular mechanisms.

Effect of cMyBP-C on Thin Filament Activation. Previous structural studies of MyBP-C binding to F-actin suggested that the N-terminal region might interfere with Tm binding to actin, especially when Tm is in its low Ca^{2+} position (25, 27, 28). We tested this proposal directly by decorating regulated thin filaments (containing Tm and Tn) with C0C2. Our results, showing clear movement of Tm from the blocked toward the closed position under low Ca^{2+} conditions, directly support the hypothesis that the N terminus of cMyBP-C competes with Tm (in its blocked position) for the same binding region on actin; this competition is further suggested by the greater movement of Tm that occurs when cMyBP-C is added to F-actin before Tm and Tn. This cMyBP-C-induced shift of Tm could straightforwardly explain the activation of thin filament sliding in the in vitro motility assay by C0C3 (Fig. 6) and C0C2 (19), the reduced Ca^{2+}-sensitivity of contraction of cardiac myocytes from cMyBP-C knockout mice (40), and the activation of myosin ATPase activity by thin filaments under low Ca^{2+} conditions when cMyBP-C N-terminal fragments are present (36, 37). Interestingly, solution ATPase assays found strong activation

even at low levels of added C1C2 (actin:C1C2 = 7:1) (37), where Tm movement in our reconstructions was small. Variations in conditions between the ATPase and EM experiments may account for this difference. For example, thin filament activation was measured by the rate of nucleotide release from thin filament-bound myosin subfragment 1 (S1), whereas S1 is absent from our experiments. Sparse decoration of thin filaments by cMyBP-C fragments may weaken Tm binding in the blocked position without significantly changing its average position observed by EM. This could increase the freedom of movement of Tm so that single S1 binding events are no longer significantly inhibited. Physiological experiments in which N-terminal fragments of cMyBP-C are diffused into skinned myocytes (46, 47) also demonstrate activation of contraction at low (relaxing) Ca^{2+} concentrations. In these experiments, it was suggested that cMyBP-C affects crossbridge cycling primarily by binding to myosin, thus affecting myosin crossbridge mechanics, although mechanisms involving actin binding were also considered possible. Our results suggest that cMyBP-C increases thin filament calcium sensitivity by binding to actin and displacing Tm toward the closed position.

The cMyBP-C domains primarily involved in binding actin appear to be the C1 and M-domains (9, 15, 16, 20), although there is evidence that C0 may be important (10, 14). Previous modeling suggested that the C0 and C1 domains could clash with Tm in its blocked position (25, 27, 28), whereas experiments in which expressed N-terminal fragments were added to skinned cardiac myocytes implicated the ProAla-rich domain between C0 and C1 in modulating Ca^{2+} activation of crossbridge cycling (46). However, in similar skinned fiber experiments, the ProAla-rich domain was found to have no effect, whereas the C1 and M-domains were critical to the Ca^{2+}-sensitizing and activating effects of various N-terminal domains (48). This too was the case in the present study, as only the N-terminal fragments containing the C1 and M-domains were able to displace Tm (C0C2) and activate the thin filament (C0C3). C0C1f (containing C0, the ProAla-rich domain, C1, and the first 17 amino acids of the M-domain; Fig. 1) was capable of binding to thin filaments at low Ca^{2+} but did not displace Tm from the blocked position and did not activate thin filament sliding. Therefore, thin filament activation by the N terminus of cMyBP-C under relaxing conditions (pCa > 7) likely involves multiple sites of interaction with actin to move Tm into the closed position. Assuming that C0C1f binds to the thin filament through the same contacts as C0C2, then additional sites of actin interaction must exist beyond the first 17 amino acids of the M-domain that are present in the C0C1f fragment. For example, arginines 279/280 (further along the M-domain) have been identified as critical to actin binding (9), and when mutated to alanines, they diminish the capacity of C1C2 fragments to activate thin filaments in skinned rat trabeculae (49).

Effect of cMyBP-C on the Inhibition of Sliding Velocity. In addition to the thin filament activating effects of cMyBP-C at low Ca^{2+}, cMyBP-C also governs contractility, as evidenced by enhanced unloaded cardiac muscle shortening velocities in cMyBP-C null mice (43). The inhibition of velocity in the presence of cMyBP-C occurs through cMyBP-C's N terminus, as observed previously by ourselves and others (16, 19, 20, 50) and confirmed here (Fig. 6). Because our structural studies demonstrate that C0C2 and C0C1f bind to the thin filament at high Ca^{2+}, inhibition of maximal sliding velocity could be explained by tethering of the thin filaments to the motility surface by the N-terminal domains, imparting a load on the actomyosin interactions (16), or by preventing myosin from interacting with the thin filament by occupying available myosin binding sites. In the intact sarcomere, MyBP-C is thought to bind by its 3 C-terminal domains to the thick filament backbone, whereas the rest of the molecule extends to adjacent thin filaments (5, 22, 51, 52). Thus, although the molar ratio of MyBP-C to actin subunits in the C-zone is only ~1:10, the proximity of its N termini to actin may make their effective local concentration high enough to bind the thin filament without substantial occupancy of S1 binding sites. With only minimal steric interference with S1 binding, the inhibition of maximal velocity would likely arise from tethering between the thick and thin filaments. However, our structural studies cannot exclude the possibility that N-terminal domains inhibit thin filament velocity in the in vitro motility assay by binding to myosin S2 (47) or the regulatory light chain (11) to alter myosin kinetics.

Conclusions

We conclude that the N-terminal region of cMyBP-C binds to F-actin at a location that directly competes with Tm in the blocked position. This competition is sufficient to displace Tm toward the closed position and activate the thin filament, providing a means of modulating the Ca^{2+} sensitivity of thin filaments in cardiac muscle. Similar modulation may also occur in skeletal muscle. In addition to activating the thin filament, cMyBP-C's N terminus can also inhibit myosin-generated thin filament sliding. However, these two distinct functions appear to occur through independent mechanisms, as emphasized by the inability of C0C1f to activate the thin filament despite retaining its inhibitory capacity, in contrast to the larger C0C2 and C0C3 fragments, which activate the thin filament (by Tm movement) while also slowing filament sliding. Although thin filament activation must be in part a result of cMyBP-C binding directly to actin, mechanical inhibition may still be through either actin and/or myosin binding. Experiments to distinguish which binding partner cMyBP-C interacts with to inhibit actomyosin interactions will be critical. We note, finally, that cMyBP-C phosphorylation in response to beta-adrenergic stimulation leads to enhanced cardiac contractility (53). Serine phosphorylation in cMyBP-C's M-domain by a host of kinases reduces the affinity of the N terminus for actin (15) and myosin (7). Therefore, modulation of cMyBP-C's binding capacity by phosphorylation may add a measure of tunability to cMyBP-C's regulation of cardiac contractility in response to physiological stress.

Materials and Methods

Detailed methods are provided in *SI Materials and Methods* and summarized here.

Proteins. F-actin was purified from chicken pectoralis muscle (54) and native thin filaments from porcine cardiac muscle (55, 56). Bovine cardiac tropomyosin and troponin were produced as previously described (57). cMyBP-C N-terminal fragments C0C1f (1–269), C0C2 (1–448), and C0C3 (1–539) were bacterially expressed as described previously (27). For the motility assays, myosin (58) and native thin filaments (59) (with modifications described in *SI Materials and Methods*) were freshly isolated from mouse hearts.

Electron Microscopy. Native thin filaments, or F-actin preincubated with tropomyosin and troponin (60), were mixed with varying ratios of C0C1f and C0C2 under different buffer conditions used in previous thin filament studies (27, 36, 37, 60). Five-microliter aliquots were applied to EM grids coated with thin carbon and negatively stained with 1% (wt/vol) uranyl acetate. Dried grids were observed in a Philips CM120 electron microscope (FEI) and low-dose images acquired at a pixel size of 0.35 nm, using a 2K × 2K CCD camera (F224HD, TVIPS GmbH).

3D Reconstruction. Thin filaments were unbent using ImageJ and selected regions converted to SPIDER format and cut into segments in SPIDER (v11.2; Wadsworth Center). Iterative helical real-space reconstruction was carried out using SPIDER (38, 61), with F-actin as an initial reference model. UCSF Chimera (62) was used for visualization, analysis, and atomic fitting of 3D volumes.

In Vitro Motility. In vitro motility assays were performed on the surface of a nitrocellulose-coated flow cell, and the motion of actin filaments was observed by epifluorescence microscopy, as previously described (63).

ACKNOWLEDGMENTS. We thank Dr. John Woodhead for discussion, Dr. Shixin Yang for help with SPIDER procedures, and Guy Kennedy from the University of Vermont Instrumentation and Model Facility for his expert microscopy design and assistance. EM work was carried out in the Core Electron Microscopy Facility at the University of Massachusetts Medical School. This work was supported by National Institutes of Health (NIH)

Grants AR034711, HL007647, HL063774, P01 HL059408, and P01 HL069779. Molecular graphics images and atomic fitting were produced using UCSF Chimera from the Resource for Biocomputing, Visualization, and Informatics at UCSF (supported by NIH Grant P41 RR-01081).

1. Offer G, Moos C, Starr R (1973) A new protein of the thick filaments of vertebrate skeletal myofibrils. Extraction, purification and characterization. *J Mol Biol* 74(4): 653–676.
2. Winegrad S (1999) Cardiac myosin binding protein C. *Circ Res* 84(10):1117–1126.
3. Barefield D, Sadayappan S (2010) Phosphorylation and function of cardiac myosin binding protein-C in health and disease. *J Mol Cell Cardiol* 48(5):866–875.
4. Craig R, Offer G (1976) The location of C-protein in rabbit skeletal muscle. *Proc R Soc Lond B Biol Sci* 192(1109):451–461.
5. Flashman E, Redwood C, Moolman-Smook J, Watkins H (2004) Cardiac myosin binding protein C: Its role in physiology and disease. *Circ Res* 94(10):1279–1289.
6. Starr R, Offer G (1978) The interaction of C-protein with heavy meromyosin and subfragment-2. *Biochem J* 171(3):813–816.
7. Gruen M, Prinz H, Gautel M (1999) cAPK-phosphorylation controls the interaction of the regulatory domain of cardiac myosin binding protein C with myosin-S2 in an on-off fashion. *FEBS Lett* 453(3):254–259.
8. Ababou A, et al. (2008) Myosin binding protein C positioned to play a key role in regulation of muscle contraction: Structure and interactions of domain C1. *J Mol Biol* 384(3):615–630.
9. Bhuiyan MS, Gulick J, Osinska H, Gupta M, Robbins J (2012) Determination of the critical residues responsible for cardiac myosin binding protein C's interactions. *J Mol Cell Cardiol* 53(6):838–847.
10. Lu Y, Kwan AH, Trewhella J, Jeffries CM (2011) The C0C1 fragment of human cardiac myosin binding protein C has common binding determinants for both actin and myosin. *J Mol Biol* 413(5):908–913.
11. Ratti J, Rostkova E, Gautel M, Pfuhl M (2011) Structure and interactions of myosin-binding protein C domain C0: Cardiac-specific regulation of myosin at its neck? *J Biol Chem* 286(14):12650–12658.
12. Moos C, Mason CM, Besterman JM, Feng IN, Dubin JH (1978) The binding of skeletal muscle C-protein to F-actin, and its relation to the interaction of actin with myosin subfragment-1. *J Mol Biol* 124(4):571–586.
13. Yamamoto K (1986) The binding of skeletal muscle C-protein to regulated actin. *FEBS Lett* 208(1):123–127.
14. Kulikovskaya I, McClellan G, Flavigny J, Carrier L, Winegrad S (2003) Effect of MyBP-C binding to actin on contractility in heart muscle. *J Gen Physiol* 122(6):761–774.
15. Shaffer JF, Kensler RW, Harris SP (2009) The myosin-binding protein C motif binds to F-actin in a phosphorylation-sensitive manner. *J Biol Chem* 284(18):12318–12327.
16. Weith A, et al. (2012) Unique single molecule binding of cardiac myosin binding protein-C to actin and phosphorylation-dependent inhibition of actomyosin motility requires 17 amino acids of the motif domain. *J Mol Cell Cardiol* 52(1):219–227.
17. Squire JM, Luther PK, Knupp C (2003) Structural evidence for the interaction of C-protein (MyBP-C) with actin and sequence identification of a possible actin-binding domain. *J Mol Biol* 331(3):713–724.
18. Rybakova IN, Greaser ML, Moss RL (2011) Myosin binding protein C interaction with actin: Characterization and mapping of the binding site. *J Biol Chem* 286(3):2008–2016.
19. Razumova MV, et al. (2006) Effects of the N-terminal domains of myosin binding protein-C in an in vitro motility assay: Evidence for long-lived cross-bridges. *J Biol Chem* 281(47):35846–35854.
20. Previs MJ, Beck Previs S, Gulick J, Robbins J, Warshaw DM (2012) Molecular mechanics of cardiac myosin-binding protein C in native thick filaments. *Science* 337(6099): 1215–1218.
21. Luther PK, Craig R (2011) Modulation of striated muscle contraction by binding of myosin binding protein C to actin. *BioArchitecture* 1(6):277–283.
22. Luther PK, et al. (2011) Direct visualization of myosin-binding protein C bridging myosin and actin filaments in intact muscle. *Proc Natl Acad Sci USA* 108(28):11423–11428.
23. Oakley CE, Chamoun J, Brown LJ, Hambly BD (2007) Myosin binding protein-C: Enigmatic regulator of cardiac contraction. *Int J Biochem Cell Biol* 39(12):2161–2166.
24. Gautel M, Zuffardi O, Freiburg A, Labeit S (1995) Phosphorylation switches specific for the cardiac isoform of myosin binding protein-C: A modulator of cardiac contraction? *EMBO J* 14(9):1952–1960.
25. Whitten AE, Jeffries CM, Harris SP, Trewhella J (2008) Cardiac myosin-binding protein C decorates F-actin: Implications for cardiac function. *Proc Natl Acad Sci USA* 105(47): 18360–18365.
26. Kensler RW, Shaffer JF, Harris SP (2011) Binding of the N-terminal fragment C0-C2 of cardiac MyBP-C to cardiac F-actin. *J Struct Biol* 174(1):44–51.
27. Mun JY, et al. (2011) Electron microscopy and 3D reconstruction of F-actin decorated with cardiac myosin-binding protein C (cMyBP-C). *J Mol Biol* 410(2):214–225.
28. Orlova A, Galkin VE, Jeffries CM, Egelman EH, Trewhella J (2011) The N-terminal domains of myosin binding protein C can bind polymorphically to F-actin. *J Mol Biol* 412(3):379–386.
29. Gordon AM, Homsher E, Regnier M (2000) Regulation of contraction in striated muscle. *Physiol Rev* 80(2):853–924.
30. Lehman W, Craig R (2008) Tropomyosin and the steric mechanism of muscle regulation. *Adv Exp Med Biol* 644:95–109.
31. Lehman W, Craig R, Vibert P (1994) Ca^{2+}-induced tropomyosin movement in Limulus thin filaments revealed by three-dimensional reconstruction. *Nature* 368(6466):65–67.
32. Vibert P, Craig R, Lehman W (1997) Steric-model for activation of muscle thin filaments. *J Mol Biol* 266(1):8–14.
33. Parry DA, Squire JM (1973) Structural role of tropomyosin in muscle regulation: Analysis of the x-ray diffraction patterns from relaxed and contracting muscles. *J Mol Biol* 75(1):33–55.
34. Huxley HE (1973) Structural changes in the actin- and myosin-containing filaments during contraction. *Cold Spring Harb Symp Quant Biol* 37:361–376.
35. Haselgrove JC (1973) X-ray evidence for a conformational change in the actin-containing filaments of vertebrate striated muscle. *Cold Spring Harb Symp Quant Biol* 37: 341–352.
36. White HD, Harris S (2012) Activation of cardiac thin filaments by N-terminal domains of cardiac myosin binding protein C. *Biophys J* 102(3):435a.
37. White HD, Belknap B, Harris SP (2013) Activation and inhibition of F-actin and cardiac thin filaments by the N-terminal domains of cardiac myosin binding protein C. *Biophys J* 104(2):158a–159a.
38. Egelman EH (2000) A robust algorithm for the reconstruction of helical filaments using single-particle methods. *Ultramicroscopy* 85(4):225–234.
39. Poole KJ, et al. (2006) A comparison of muscle thin filament models obtained from electron microscopy reconstructions and low-angle X-ray fibre diagrams from non-overlap muscle. *J Struct Biol* 155(2):273–284.
40. Harris SP, et al. (2002) Hypertrophic cardiomyopathy in cardiac myosin binding protein-C knockout mice. *Circ Res* 90(5):594–601.
41. Korte FS, McDonald KS, Harris SP, Moss RL (2003) Loaded shortening, power output, and rate of force redevelopment are increased with knockout of cardiac myosin binding protein-C. *Circ Res* 93(8):752–758.
42. Hofmann PA, Hartzell HC, Moss RL (1991) Alterations in Ca^{2+} sensitive tension due to partial extraction of C-protein from rat skinned cardiac myocytes and rabbit skeletal muscle fibers. *J Gen Physiol* 97(6):1141–1163.
43. Palmer BM, et al. (2004) Role of cardiac myosin binding protein C in sustaining left ventricular systolic stiffening. *Circ Res* 94(9):1249–1255.
44. Hofmann PA, Greaser ML, Moss RL (1991) C-protein limits shortening velocity of rabbit skeletal muscle fibres at low levels of Ca^{2+} activation. *J Physiol* 439:701–715.
45. Stelzer JE, Dunning SB, Moss RL (2006) Ablation of cardiac myosin-binding protein-C accelerates stretch activation in murine skinned myocardium. *Circ Res* 98(9):1212–1218.
46. Herron TJ, et al. (2006) Activation of myocardial contraction by the N-terminal domains of myosin binding protein-C. *Circ Res* 98(10):1290–1298.
47. Kunst G, et al. (2000) Myosin binding protein C, a phosphorylation-dependent force regulator in muscle that controls the attachment of myosin heads by its interaction with myosin S2. *Circ Res* 86(1):51–58.
48. Razumova MV, Bezold KL, Tu AY, Regnier M, Harris SP (2008) Contribution of the myosin binding protein C motif to functional effects in permeabilized rat trabeculae. *J Gen Physiol* 132(5):575–585.
49. Bezold KL, Shaffer JF, Khosa JK, Hoye ER, Harris SP (2013) A gain-of-function mutation in the M-domain of cardiac myosin-binding protein-C increases binding to actin. *J Biol Chem* 288(30):21496–21505.
50. Shaffer JF, Razumova MV, Tu AY, Regnier M, Harris SP (2007) Myosin S2 is not required for effects of myosin binding protein-C on motility. *FEBS Lett* 581(7): 1501–1504.
51. Zoghbi ME, Woodhead JL, Moss RL, Craig R (2008) Three-dimensional structure of vertebrate cardiac muscle myosin filaments. *Proc Natl Acad Sci USA* 105(7):2386–2390.
52. Lee K, Sadayappan S, Harris S, Craig R (2013) Determination of MyBP-C orientation in the cardiac sarcomere by immuno-EM. *Biophys J* 104(2):309a.
53. Tong CW, Stelzer JE, Greaser ML, Powers PA, Moss RL (2008) Acceleration of cross-bridge kinetics by protein kinase A phosphorylation of cardiac myosin binding protein C modulates cardiac function. *Circ Res* 103(9):974–982.
54. Pardee JD, Spudich JA (1982) Purification of muscle actin. *Methods Enzymol* 85(Pt B): 164–181.
55. Spiess M, et al. (1999) Isolation, electron microscopic imaging, and 3-D visualization of native cardiac thin myofilaments. *J Struct Biol* 126(2):98–104.
56. Matsumoto F, et al. (2004) Conformational changes of troponin C within the thin filaments detected by neutron scattering. *J Mol Biol* 342(4):1209–1221.
57. Tobacman LS, Adelstein RS (1986) Mechanism of regulation of cardiac actin-myosin subfragment 1 by troponin-tropomyosin. *Biochemistry* 25(4):798–802.
58. Debold EP, et al. (2007) Hypertrophic and dilated cardiomyopathy mutations differentially affect the molecular force generation of mouse alpha-cardiac myosin in the laser trap assay. *Am J Physiol Heart Circ Physiol* 293(1):H284–H291.
59. Lehman W, Vibert P, Uman P, Craig R (1995) Steric-blocking by tropomyosin visualized in relaxed vertebrate muscle thin filaments. *J Mol Biol* 251(2):191–196.
60. Pirani A, et al. (2005) Single particle analysis of relaxed and activated muscle thin filaments. *J Mol Biol* 346(3):761–772.
61. Frank J, et al. (1996) SPIDER and WEB: Processing and visualization of images in 3D electron microscopy and related fields. *J Struct Biol* 116(1):190–199.
62. Pettersen EF, et al. (2004) UCSF Chimera—a visualization system for exploratory research and analysis. *J Comput Chem* 25(13):1605–1612.
63. Palmiter KA, et al. (2000) R403Q and L908V mutant beta-cardiac myosin from patients with familial hypertrophic cardiomyopathy exhibit enhanced mechanical performance at the single molecule level. *J Muscle Res Cell Motil* 21(7):609–620.

Supporting Information

Mun et al. 10.1073/pnas.1316001111

SI Materials and Methods

Proteins. F-actin was purified from chicken pectoralis muscle (1). Native thin filaments were purified from porcine cardiac muscle according to Spiess (2), as modified by Matsumoto (3). Bovine cardiac tropomyosin and troponin were produced as described by Tobacman and Adelstein (4). cMyBP-C N-terminal fragments C0C1f (1–269), C0C2 (1–448), and C0C3 (1–539) were bacterially expressed and purified from mouse cardiac cDNA, using the pET expression system (Novagen), as described previously (5).

For the in vitro motility assays, myosin and native thin filaments were freshly isolated from mouse hearts. All protocols complied with the Guide for the Use and Care of Laboratory Animals published by the National Institutes of Health and were approved by the institutional animal care and use committees at University of Vermont Medical School. Wild-type mice of the FVB strain were killed by cervical dislocation. The apex of the heart was removed and was cut into two ∼30-mg pieces. Monomeric myosin was isolated from one piece of the muscle, as previously described (6), and native thin filaments were isolated from the other piece of muscle as follows.

For native mouse cardiac thin filaments, the muscle was immediately placed into a 1.5-mL tube containing 1 mL chilled relaxing solution (50 mM NaCl, 5 mM $MgCl_2$, 2 mM EGTA, 1 mM DTT, 7 mM phosphate buffer at pH 7, 10 mM creatine phosphate, 2.5 mM ATP) and agitated for 1 min by shaking (7). The muscle was transferred with tweezers (Dumont #5, Biologie Tips) to a dissecting chamber containing 1 mL chilled relaxing solution with 0.5% Triton-X 100 and then teased into 3–5-mm strips, using the tweezers. The muscle strips were transferred with the tweezers into a 0.2-mL glass tissue homogenizer (Kontes, Fisher Scientific) containing 150 μL homogenization buffer (100 mM KCl, 5 mM $MgCl_2$, 1 mM EGTA, 25 mM imidazole at pH 6.45, 10 mM DTT, 5 mM ATP, and 0.1% Triton X-100) and homogenized on ice for 15 min. The homogenate was centrifuged in a TLA-100 rotor (Beckman, Coulter) (20 min, 40,000 × *g*). The supernatant was transferred into a new centrifuge tube and recentrifuged (45 min, 200,000 × *g*). The supernatant was discarded; the pellet was resuspended in 75 μL of 100 mM KCl, 5 mM $MgCl_2$, 1 mM EGTA, 25 mM imidazole (pH 7.9), 10 mM DTT, and 5 mM ATP; and the suspension was centrifuged (5 min, 40,000 × *g*). The supernatant was transferred to a new centrifuge tube and recentrifuged (45 min, 200,000 × *g*). The pellet, which contained the native thin filaments, was softened overnight with 10 μL homogenization buffer without ATP or Triton X-100. The following morning, the total protein concentration was determined using a Bradford assay (Bio-Rad), and the actin concentration was estimated from the total protein content, assuming the presence of 7 actin monomers per troponin and tropomyosin complex. The native thin filaments were fluorescently labeled by mixing 10 μM actin with 10 μM tetramethyl-rhodamine-phalloidin in homogenization buffer without ATP or Triton X-100 (ice, 1 h). The labeled native thin filaments were diluted to 5 nM in actin buffer (AB) [25 mM KCl, 1 mM EGTA, 10 mM DTT, 25 mM imidazole, 4 mM $MgCl_2$, adjusted to pH 7.4; containing an oxygen scavenging system (0.1 μg/mL glucose oxidase, 0.018 μg/mL catalase, 2.3 μg/mL glucose)] before use.

Electron Microscopy. Two micromolar native thin filaments, or 2 μM F-actin preincubated with tropomyosin and troponin (7:2:2 = F-actin:Tm:Tn) (8) were mixed with 0.3–12 μM C0C2 (1:6, 1:3, 1:1, or 7:1 ratio = actin subunits: C0C2) under three different buffer conditions, each of which has been used in previous thin filament studies. The major difference between them was the KAc/NaCl concentration, and hence the ionic strength (1). One hundred millimolar KAcetate, 2 mM $MgCl_2$, 0.2 mM EGTA, 1 mM DTT, 10 mM Mops at pH 7.0 (9); (2) 100 mM NaCl, 3 mM $MgCl_2$, 0.2 mM EGTA, 1 mM NaN_3, 5 mM sodium phosphate, 5 mM Pipes at pH 7.1 (5, 8); (3) 180 mM KAcetate, 2 mM $MgCl_2$, 0.2 mM EGTA, 1 mM DTT, 10 mM Mops at pH 7.0 (10). After mixing, solutions were incubated at room temperature for 30 min. For high Ca^{2+} conditions, 0.33 mM $CaCl_2$ was added to the appropriate buffer. Five-microliter aliquots were then applied to EM grids coated with thin carbon supported by a holey carbon film and negatively stained with 1% (wt/vol) uranyl acetate (11). Dried grids were observed in a Philips CM120 electron microscope (FEI) at 80 KV under low-dose conditions. Images of filaments were acquired at a pixel size of 0.35 nm, using a 2K × 2K CCD camera (F224HD, TVIPS GmbH).

3D Reconstruction. Long, relatively straight thin filaments were chosen for 3D reconstruction and unbent using ImageJ. Selected filament regions were converted to SPIDER format (EM2EM; Image Science and Imperial College, London, United Kingdom), and cut into segments in SPIDER (v11.2; Wadsworth Center). Iterative helical real-space reconstruction was carried out using SPIDER (12, 13). An F-actin model (no tropomyosin) was used as an initial reference model for the first round of iterative helical real-space reconstruction so that the model would not bias the position of Tm in the reconstruction (similar results were obtained using a uniform cylinder as the reference). Filament segments were fitted to different rotational views of the reference represented by 90 2D projections of the model turned 360° in 4° intervals. Cross-correlation and alignment were performed between the filament segments and the projections, using the AP NQ routine in SPIDER. Segments aligning with incorrect polarity or with in-plane rotations greater than ± 4° from their preset vertical orientation were discarded, and the remaining segments were back-projected using the SPIDER BP 3F routine. A search for helical symmetry was performed, and the symmetrized reconstruction was used as a reference model for the next round of alignment and image reconstruction (13). The process was iterated for 20 rounds, with convergence (no changes from one round to the next) generally occurring within 10 rounds. The resulting reconstructions had resolutions between 1.6 and 3.2 nm, according to the Fourier shell correlation 0.5 criterion, with the higher resolutions being obtained for the undecorated filaments. UCSF Chimera (14) was used for visualization, analysis, and atomic fitting of 3D volumes.

Comparison and Atomic Fitting of Reconstructions. Accurate matching of reconstructions to each other was essential to determine whether cMyBP-C N-terminal fragments caused tropomyosin movement. Matching was carried out using an F-actin reconstruction as a reference to which all other reconstructions were fitted. This matching was done using the highest-density region of actin in both the experimental and reference F-actin structures (the SD1 region in all cases) as the guide to the superposition. After adjusting the two reconstructions to a high-contour cutoff, an approximate fit was carried out manually; this was then optimized using the "fit in map" tool of Chimera, which shifts and rotates the reconstruction relative to the F-actin reference to maximize their correlation. Using this approach, only the densities greater than or equal to the high-contour cutoff selected are used for matching; the

lower-density tropomyosin and C0C2 contributions are ignored and do not influence the fitting. After fitting, the contour cutoff was lowered so that tropomyosin and the outer surface of F-actin in the experimental reconstruction became visible. Comparison of different experimental reconstructions, all fitted to the same reference F-actin model, revealed any changes in tropomyosin position. The same fitting was obtained using a variety of different high-contour cutoffs, showing that the exact choice of cutoff was not critical. Comparison of control low and high Ca^{2+} filaments shows that this approach works by demonstrating the known shift of tropomyosin in response to Ca^{2+} (Fig. 3).

The reconstructions were fitted with atomic models of F-actin and/or F-actin-tropomyosin determined by X-ray diffraction and cryo-EM (15, 16). First, the reconstruction of F-actin alone was fitted to the F-actin atomic model, using the Chimera "fit in map" tool, as described earlier. A surface contour of the reconstruction was then chosen that enclosed the atomic model with minimal projection of actin density outside of the envelope. To compare the positions of the tropomyosin strands in the experimental reconstructions with the known high and low Ca^{2+} positions of tropomyosin in the atomic model, the experimental reconstruction was made translucent and the atomic model (fitted to F-actin as above) was made visible within it, revealing the position of tropomyosin in the atomic model (e.g., Figs. 3 *A* and *B* and 4 *A*–*C*). Because all reconstructions were fitted to the same reference F-actin model, the atomic fitting was standardized across all reconstructions.

In Vitro Motility. In vitro motility assays were performed on the surface of a nitrocellulose-coated flow cell, and the motion of actin filaments was observed by epifluorescence microscopy, similar to that previously described (17). In short, 100 μg/mL mouse cardiac myosin was incubated in the flow cell (2 min), and then the surface of the flow cell was blocked by the addition of two aliquots of BSA (1 mg/mL in AB). Next, two aliquots of 1 μM unlabeled native thin filaments in AB were added to the flow cell (1 min). The flow cell was rinsed two times with 1 mM ATP in AB to eliminate myosin that irreversibly binds actin in an ATP-insensitive manner (17), and then two more times with AB. Two aliquots of tetramethyl-rhodamine-phalloidin-labeled native thin filaments were added to the flow cell (1 min), and then the flow cell was rinsed three times with AB. Motility buffer [AB containing 100 μM ATP, 0.5% methyl cellulose, calcium chloride ranging from negative log of calcium concentration (pCa) 4–9, and 1 μM of either C0C1f or C0C3 (where applicable)] was added to the flow cell, and actin filament motion was observed by epifluorescence microscopy at 22 °C after 3 min incubation. Calcium levels were determined using MaxChelator software (18) to account for the 1 mM EGTA present in the motility buffer.

A Lumen 200W metal arc lamp (Prior Scientific) was used for fluorescent excitation, a Nikon Eclipse Ti-U microscope equipped with a PlanApo objective lens (100×, 1.35 n.a.) and an intensified high-resolution Mega Z 10-bit digital camera (Stanford Photonics), using Piper software, were used to acquire the images at 10 frames/s without pixel binning (95 nm/pixel). The image stacks were down-sampled to 2 frames/s, using Image J 1.43u (National Institutes of Health), and DiaTrack 3.03 software for Windows (Semasopht) was used for data analysis. The velocity of each moving actin filament and percentage of motile filaments were determined in each movie. The mean velocity and fraction moving were determined from four movies for each experimental condition, and the product was determined. The mean velocity × fraction of moving filaments ± SEM from three independent experiments were determined. Velocity × fraction of moving filaments were plotted with respect to pCa, fitted with a sigmoidal dose–response curve, and the pCa_{50} used to determine changes in calcium sensitivity.

1. Pardee JD, Spudich JA (1982) Purification of muscle actin. *Methods Enzymol* 85(Pt B): 164–181.
2. Spiess M, et al. (1999) Isolation, electron microscopic imaging, and 3-D visualization of native cardiac thin myofilaments. *J Struct Biol* 126(2):98–104.
3. Matsumoto F, et al. (2004) Conformational changes of troponin C within the thin filaments detected by neutron scattering. *J Mol Biol* 342(4):1209–1221.
4. Tobacman LS, Adelstein RS (1986) Mechanism of regulation of cardiac actin-myosin subfragment 1 by troponin-tropomyosin. *Biochemistry* 25(4):798–802.
5. Mun JY, et al. (2011) Electron microscopy and 3D reconstruction of F-actin decorated with cardiac myosin-binding protein C (cMyBP-C). *J Mol Biol* 410(2): 214–225.
6. Debold EP, et al. (2007) Hypertrophic and dilated cardiomyopathy mutations differentially affect the molecular force generation of mouse alpha-cardiac myosin in the laser trap assay. *Am J Physiol Heart Circ Physiol* 293(1):H284–H291.
7. Lehman W, Vibert P, Uman P, Craig R (1995) Steric-blocking by tropomyosin visualized in relaxed vertebrate muscle thin filaments. *J Mol Biol* 251(2):191–196.
8. Pirani A, et al. (2005) Single particle analysis of relaxed and activated muscle thin filaments. *J Mol Biol* 346(3):761–772.
9. White HD, Belknap B, Harris SP (2013) Activation and inhibition of F-actin and cardiac thin filaments by the N-terminal domains of cardiac myosin binding protein C. *Biophys J* 104(2):158a–159a.
10. White HD, Harris S (2012) Activation of cardiac thin filaments by N-terminal domains of cardiac myosin binding protein C. *Biophys J* 102(3):435a.
11. Craig R, Lehman W (2001) Crossbridge and tropomyosin positions observed in native, interacting thick and thin filaments. *J Mol Biol* 311(5):1027–1036.
12. Frank J, et al. (1996) SPIDER and WEB: Processing and visualization of images in 3D electron microscopy and related fields. *J Struct Biol* 116(1):190–199.
13. Egelman EH (2000) A robust algorithm for the reconstruction of helical filaments using single-particle methods. *Ultramicroscopy* 85(4):225–234.
14. Pettersen EF, et al. (2004) UCSF Chimera—a visualization system for exploratory research and analysis. *J Comput Chem* 25(13):1605–1612.
15. Holmes KC, Angert I, Kull FJ, Jahn W, Schröder RR (2003) Electron cryo-microscopy shows how strong binding of myosin to actin releases nucleotide. *Nature* 425(6956): 423–427.
16. Poole KJ, et al. (2006) A comparison of muscle thin filament models obtained from electron microscopy reconstructions and low-angle X-ray fibre diagrams from non-overlap muscle. *J Struct Biol* 155(2):273–284.
17. Palmiter KA, et al. (2000) R403Q and L908V mutant beta-cardiac myosin from patients with familial hypertrophic cardiomyopathy exhibit enhanced mechanical performance at the single molecule level. *J Muscle Res Cell Motil* 21(7):609–620.
18. Patton C, Thompson S, Epel D (2004) Some precautions in using chelators to buffer metals in biological solutions. *Cell Calcium* 35(5):427–431.

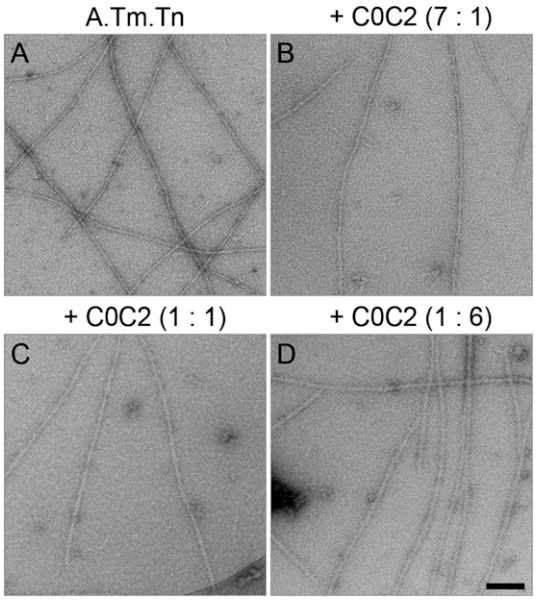

Fig. S1. Comparison of reconstituted thin filaments decorated with different ratios of C0C2 in low Ca^{2+} conditions. (*A*) Thin filament control. (*B–D*) Filaments decorated with C0C2 at the A:C0C2 molar ratios indicated. (Scale bar = 100 nm.)

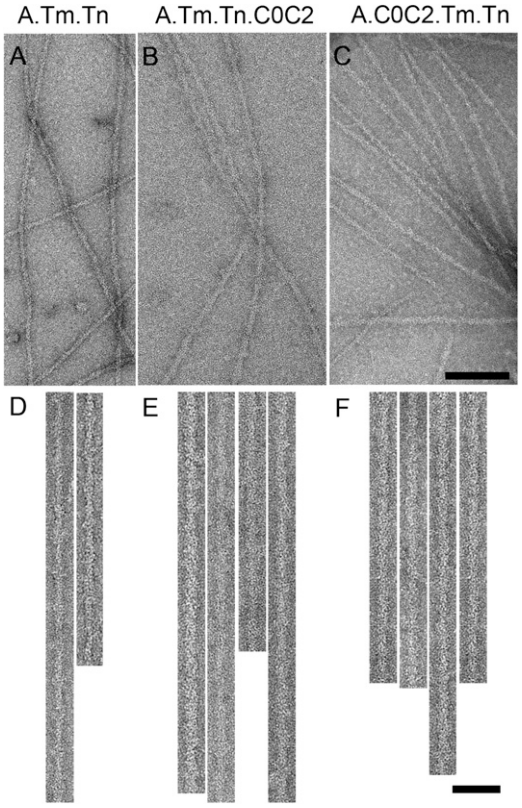

Fig. S2. Decoration of low Ca^{2+} reconstituted thin filaments using different mixing orders. (*A*, *D*) Reconstituted thin filament control. (*B*, *C*, *E*, *F*) Filaments decorated with C0C2, added after (*B*, *E*) or before (*C*, *F*) Tm.Tn. Filaments in *D–F* have been computationally straightened. [Scale bar (*A–C*) = 100 nm; (*D–F*) = 50 nm.]

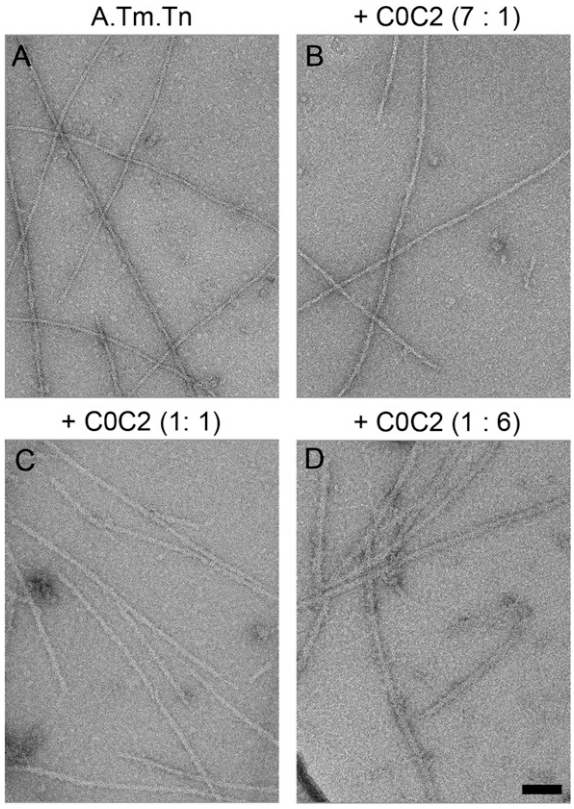

Fig. S3. Comparison of C0C2-decorated thin filaments under high Ca^{2+} conditions at different A:C0C2 ratios. (*A*) Thin filament control; (*B–D*) Filaments decorated with C0C2 at the ratios indicated. (Scale bar = 50 nm.)

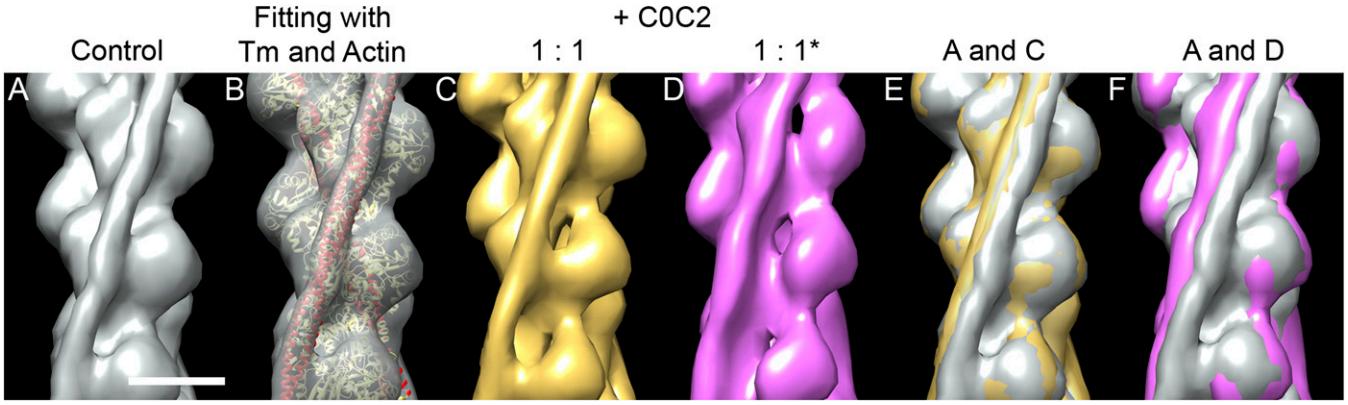

Fig. S4. 3D reconstructions of low Ca^{2+} reconstituted thin filaments decorated with C0C2 in different mixing orders. (*A*) Undecorated (control) filament. (*B*) Control filament fitted with ribbon depiction of F-actin. Tm atomic model in blocked state (actin monomers, yellow; Tm, red). (*C*) C0C2-decorated thin filament (A:C0C2 = 1:1), showing small shift of Tm as with native thin filaments (Fig. 4*B*). (*D*) When C0C2 was bound to actin before addition of Tm and Tn, Tm was shifted further, to approximately the closed position. (*E*, *F*) Superposition of *A* on *C*, and *A* on *D*, showing small movement (*E*) and large movement (*F*). (Scale bar = 5 nm.)

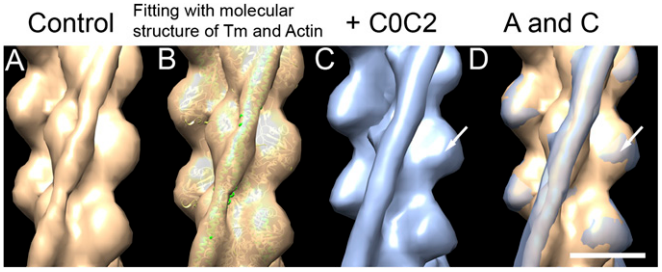

Fig. S5. 3D reconstructions of reconstituted thin filaments decorated with C0C2 under high Ca^{2+} conditions. (*A*) Undecorated (control) filament. (*B*) Control filament fitted with ribbon depiction of an F-actin. Tm atomic model in closed state (actin monomers, yellow; Tm, green). (*C*) C0C2-decorated thin filament (A:C0C2 = 1:3). (*D*) Superposition of *A* and *C*, showing little movement of Tm, which is located in both structures in the closed position. Extra density on SD1 of *C* (arrows in *C* and *D*) is presumably the proximal end of the bound C0C2. (Scale bar = 5 nm.)

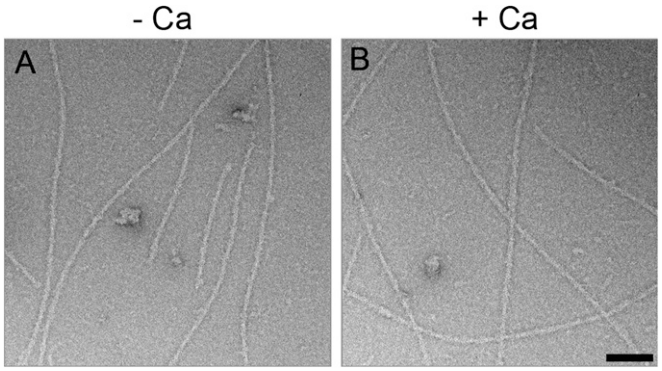

Fig. S6. Negative staining of C0C1f-decorated native thin filaments under low and high Ca^{2+} conditions at a 1:6 ratio of A:C0C2. (*A*) Low Ca^{2+} conditions. (*B*) High Ca^{2+} conditions. Both show wider filaments compared with control native thin filaments (Fig. 2*A*). (Scale bar = 100 nm.)

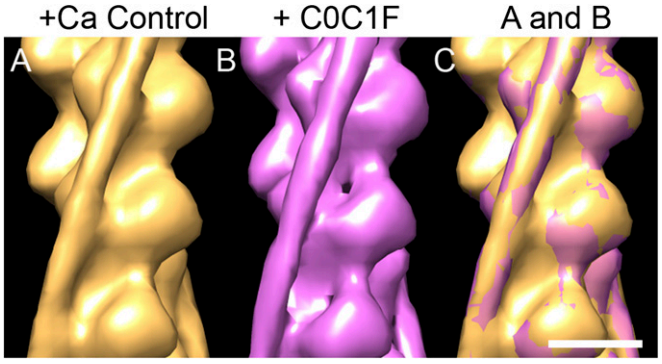

Fig. S7. 3D reconstructions of native thin filaments decorated with C0C1f under high Ca^{2+} conditions. (*A*) High Ca^{2+} control filament (yellow surface rendering). (*B*) C0C1f-decorated filament (pink). (*C*) Superposition of *A* and *B*, showing no Tm shift. (Scale bar = 5 nm.)

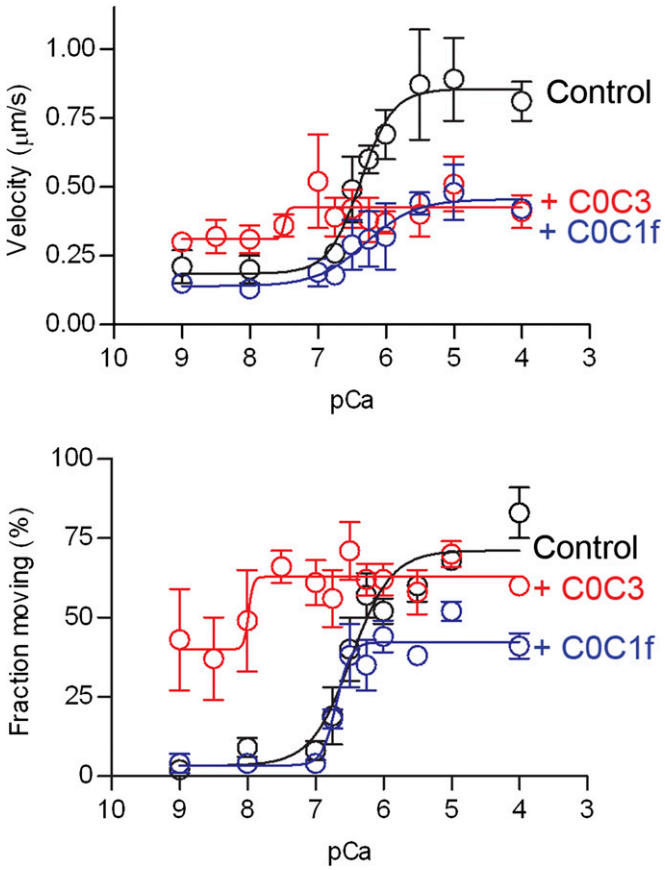

Fig. S8. Effect of N-terminal fragments on native thin filament pCa:velocity and pCa:fraction moving relations in in vitro motility assays. The black line shows native thin filaments demonstrating a sigmoidal response to Ca^{2+} in both velocity (*Upper*) and fraction of filaments moving (*Lower*). The red line shows that the presence of C0C3 increased the velocity and fraction of filaments moving at low Ca^{2+} but had a greater effect on the reduction of velocity than on the fraction of filaments moving at high Ca^{2+}. The blue line shows that the presence of C0C1f had no effect at low Ca^{2+} but reduced both the velocity and fraction of filaments moving at high Ca^{2+}. These results are summarized in Fig. 6, which shows effective activation (velocity × fraction moving vs. pCa).

Table S1. Diameters (nm) of thin filaments with or without C0C1f or C0C2 decoration (low Ca^{2+} conditions)

	Control	+ C0C2 (7: 1)	+ C0C2 (1: 1)		+ C0C2 (1: 3)	+ C0C2 (1: 6)	+ C0C1f (1: 6)
Reconstituted A.Tm.Tn	10.3 ± 0.7	11.6 ± 0.6	14.4 ± 1.3	14.3 ± 0.4*	17.1 ± 1.3	19.7 ± 1.3	15.5 ± 1.6
Native thin filament	10.5 ± 0.8	11.7 ± 1.0	14.5 ± 1.0		17.2 ± 0.7	20.1 ± 1.3	15.5 ± 1.5

Values are mean ± SD based on 20 of the filaments that had been selected for each reconstruction. For calculation of diameter, the SPIDER software package was used to obtain a density projection along the filament (after straightening). The diameter was calculated from the distance between the minima in the projection profile.

*In this experiment, C0C2 was mixed with F-actin, followed by Tm and Tn (in all other experiments, C0C2 was added to preformed thin filaments).